THREE-DIMENSIONAL SIMULATION OF A SHOCK-INDUCED BUBBLE COLLAPSE

E. GONCALVES[1] AND P. PARNAUDEAU[1]

[1] Institut Pprime, UPR 3346 CNRS, ISAE-ENSMA, Université de Poitiers
1 avenue Clement Ader, 86961 Chasseneuil cedex, France
eric.goncalves@ensma.fr and philippe.parnaudeau@univ-poitiers.fr

Key words: Shock-bubble interaction, one-fluid simulation, blast wave, jet formation

Abstract. The investigation of the pressure developed by a collapsing cavitation bubble is of primary interest for hydraulic turbomachineries, fuel injectors, naval propulsion systems and biomedical technologies. One of the most critical consequences is the shock wave emitted by bubbles collapse and the structural damage resulting when this process takes place close to solid walls. This paper presents a numerical study of the interaction between a planar incident shock wave with a gas bubble. Simulations are performed using an inviscid compressible one-fluid solver composed by three conservation laws for mixture variables, namely mass, momentum and total energy along with a supplementary transport equation for the volume fraction of the gas phase.

1 INTRODUCTION

Cavitation erosion is a major problem for hydraulic and marine applications. This phenomenon occurs when vapor bubbles collapse in the vicinity of solid walls leading to negative consequences, such as vibrations, material damages and performance loss. To clarify the physical mechanism, numerous experimental and numerical studies of the collapse of cavity in water under shock wave loading have been proposed [10, 1, 11, 5, 4, 9]. The bubble collapse close to the wall has been addressed as the fundamental mechanism producing damage. Its general behavior is characterized by the formation of a water jet that penetrates through the bubble and the generation of a blast wave during the induced collapse. Both the jet and the blast wave are possible damaging mechanisms.
In the present study, the shock induced collapse of a gas bubble located near a wall is numerically investigated. We describe the main characteristics of the phenomenon with particular consideration of the maximum wall pressure. A key parameter is the distance between the bubble center and the wall. Simulations are performed using an inviscid compressible one-fluid code based on a four-equation system. It consists in solving three mixture conservation laws for the mass, momentum and energy and a transport-equation for the gas volume fraction [2, 3].

2   EQUATIONS AND MODELS

The homogeneous mixture approach is used with the assumption of thermal and mechanical local equilibrium between pure phases. We consider a reduction of the five-equation model of Kapila [6]. The model consists in three conservation laws for mixture mass, mixture momentum and total energy together with an additional equation for the void ratio [2]. The expression for the void ratio equation α is given by:

$$\frac{\partial \rho}{\partial t} + \operatorname{div}(\vec{V}) = 0 \tag{1}$$

$$\frac{\partial (\rho \vec{V})}{\partial t} + \operatorname{div}(\rho \vec{V} \otimes \vec{V} + P I_{\mathrm{d}}) = 0 \tag{2}$$

$$\frac{\partial (\rho E)}{\partial t} + \operatorname{div}(\rho \vec{V} H) = 0 \tag{3}$$

$$\frac{\partial \alpha}{\partial t} + \operatorname{div}(\alpha \vec{V}) = \left(\underbrace{\frac{\rho_l c_l^2 - \rho_v c_v^2}{\frac{\rho_l c_l^2}{1-\alpha} + \frac{\rho_v c_v^2}{\alpha}}}_{=K} + \alpha \right) \operatorname{div}(\vec{V}) \tag{4}$$

where c_k are the speed of sound of phase k and $\vec{V}$ the mixture velocity vector. The system has a hyperbolic nature with eigenvalues: $u - c_{wallis}, u, u, u + c_{wallis}$, where c_{wallis} is the the propagation of acoustic waves without mass and heat transfer. This speed of sound is expressed as a weighted harmonic mean of speeds of sound of each phase:

$$\frac{1}{\rho c_{wallis}^2} = \frac{\alpha}{\rho_v c_v^2} + \frac{1 - \alpha}{\rho_l c_l^2} \tag{5}$$

The stiffened gas EOS is used for both pure phases. From the thermal and mechanical equilibrium assumption, an expression for the mixture pressure and temperature can be deduced :

$$P(\rho, e, \alpha, Y) = (\gamma(\alpha) - 1)\rho(e - q(Y)) - \gamma(\alpha) P_\infty(\alpha) \tag{6}$$

$$\frac{1}{\gamma(\alpha) - 1} = \frac{\alpha}{\gamma_v - 1} + \frac{1 - \alpha}{\gamma_l - 1} \quad ; \quad q(Y) = Y q_v + (1 - Y) q_l \tag{7}$$

$$P_\infty(\alpha) = \frac{\gamma(\alpha) - 1}{\gamma(\alpha)} \left[\alpha \frac{\gamma_v}{\gamma_v - 1} P_\infty^v + (1 - \alpha) \frac{\gamma_l}{\gamma_l - 1} P_\infty^l \right] \tag{8}$$

$$T(\rho, h, Y) = \frac{h - q(Y)}{C_p(Y)} \quad \text{with} \quad C_p(Y) = Y C_{p_v} + (1 - Y) C_{p_l} \tag{9}$$

where $Y = \alpha \rho_v / \rho$ is the mass fraction of gas, $\gamma = C_p / C_v$ is the heat capacity ratio, C_p and C_v are thermal capacities, q the energy of formation of the fluid and and P_∞ is a constant reference pressure.

3   NUMERICS

Numerical simulations are carried out using an in-house finite volume code solving the compressible inviscid system [3]. Numerical fluxes are computed with a HLLC scheme. The second-order is obtained through the MUSCL extrapolation and the minmod slope limiter is used. The explicit time integration is performed using a 3-step Runge-Kutta method. The numerical treatment of the boundary conditions is based on the inviscid characteristic relations.

4   PRELIMINARY RESULTS

The considered test is similar to the one presented in [8]. A cylindrical air bubble, 6 mm in diameter, is immersed in a water pool, under the following initial conditions: $\vec{V} = (0,0)$ m/s, $P = 10^5$ Pa, $\rho_{air} = 1$ kg/m^3 and $\rho_{water} = 1000$ kg/m^3. Due to the symmetry of the problem, we only consider a half bubble. The center of the bubble is located at $(9,0)$ mm in the computational domain of size 24×12 mm. The bubble is collapsed by a normal shock wave moving at $M_{sh} = 1.72$, initially located at abscissa $x_{sh} = 4$ mm. Parameters of the EOSs and post-shock conditions are:

$$\begin{pmatrix} \gamma \\ P_\infty \\ \rho \end{pmatrix}_l = \begin{pmatrix} 4.4 \\ 6.\,10^8 \\ 1000 \end{pmatrix} \quad ; \quad \begin{pmatrix} \gamma \\ P_\infty \\ \rho \end{pmatrix}_v = \begin{pmatrix} 1.4 \\ 0 \\ 1 \end{pmatrix} \quad ; \quad \begin{pmatrix} P \\ \rho \\ u \end{pmatrix}_{sh} = \begin{pmatrix} 1.9\,10^9 \\ 1323.65 \\ 681.58 \end{pmatrix}$$

The schematic diagram of the test case is given in Figure 1 (left part).
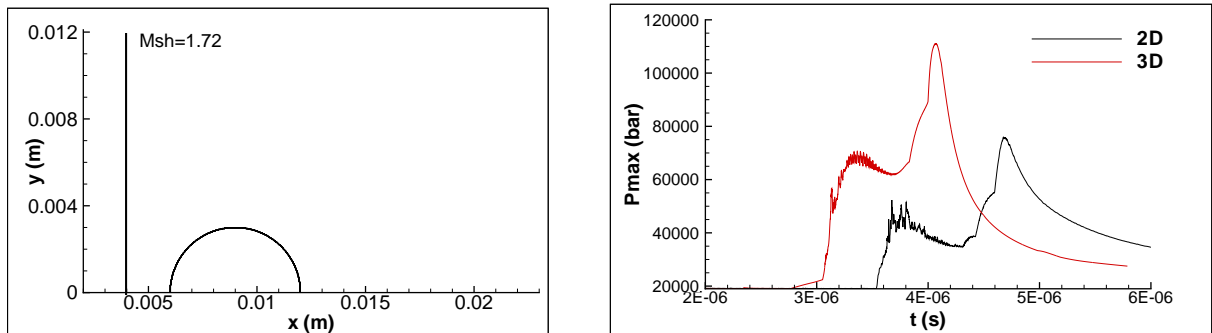
Figure 1: Initial situation for the bubble collapse (left) and evolution of the maximum pressure P_{max} during the bubble collapse (right).

Two-dimensional simulations are performed using an uniform 1200×600 mesh cells and a time step $\Delta t = 10^{-9}$ s. For the three-dimensional case, the mesh is extruded in the spanwise direction and is composed of $1200 \times 600 \times 600$ cells.

The evolution of the density gradient modulus (Schlieren-type representation) and the pressure (in bar) are plotted in Figure 2 at different instants for the 2D collapse. After the water shock wave has collided with the bubble, a strong rarefaction wave is reflected backwards from the interface, and a weak shock wave is transmitted inside of

the bubble (time $t = 2\mu$ s). Due to the pressure difference between both sides, the bubble is asymmetrically contracted and spreads laterally in the process, which induces a jet of water along the axis of flow symmetry. When this water jet impacts the right interface of the bubble (at time $t=3.6\ \mu s$), an intense blast wave is formed generating a high-pressure zone. The blast front, which expands continuously, is highly asymmetric due to the high-speed water jet (see Figure 2 at time $t = 4.2\mu$ s). The interaction of the leftward front wave with the bubble fragments lead to high pressure levels (at time $t=4.8\ \mu s$).
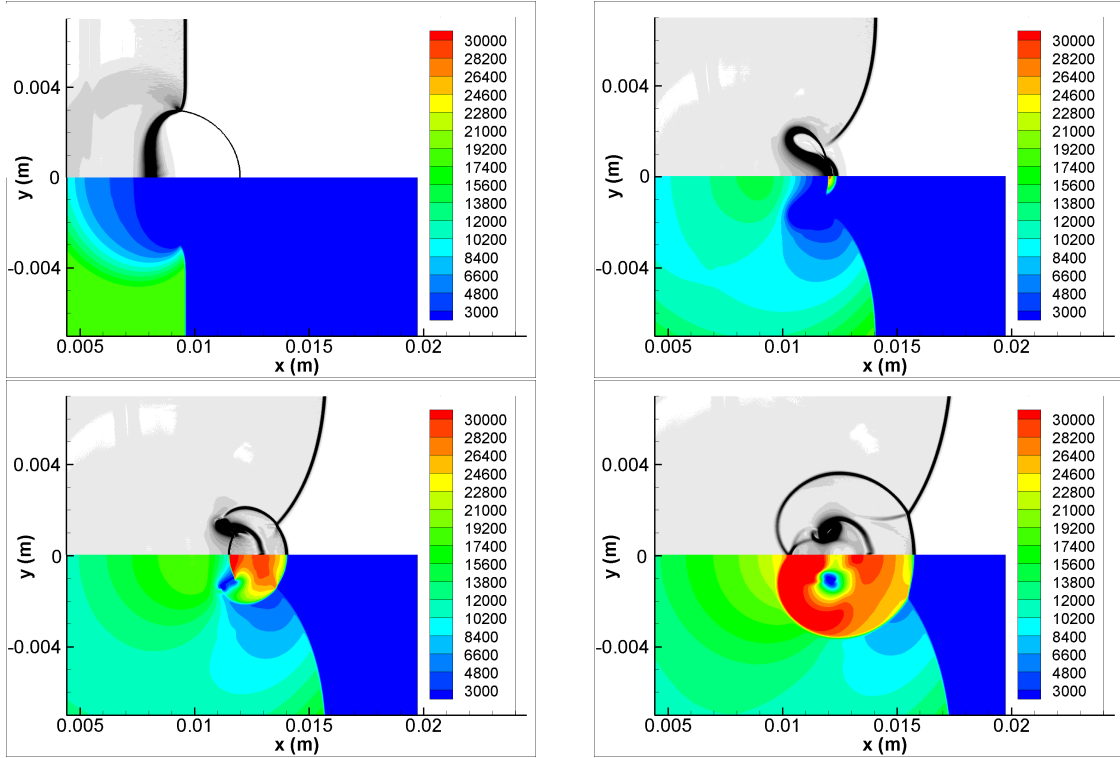
Figure 2: Evolution of the density gradient modulus and the pressure (in bar) at times $t=2$, 3.6, 4.2 and 4.8 μs. 2D simulation.

Table 1: Comparison of results from 2D and 3D simulations

	2D	3D
first peak time (μs)	3.8	3.4
first peak intensity (bar)	40000	69000
second peak time (μs)	4.7	4.1
second peak intensity (bar)	70000	110000

The pressure evolution for the 3D collapse are illustrated in Figure 3 at different instants. The jet penetration inside the bubble and the toroidal shape are clearly illustrated.

4

The jet impacts the bubble interface generating the intense blast wave. The blast fronts propagate in both direction and the leftward front collides the bubble pieces leading to a high-pressure peak.
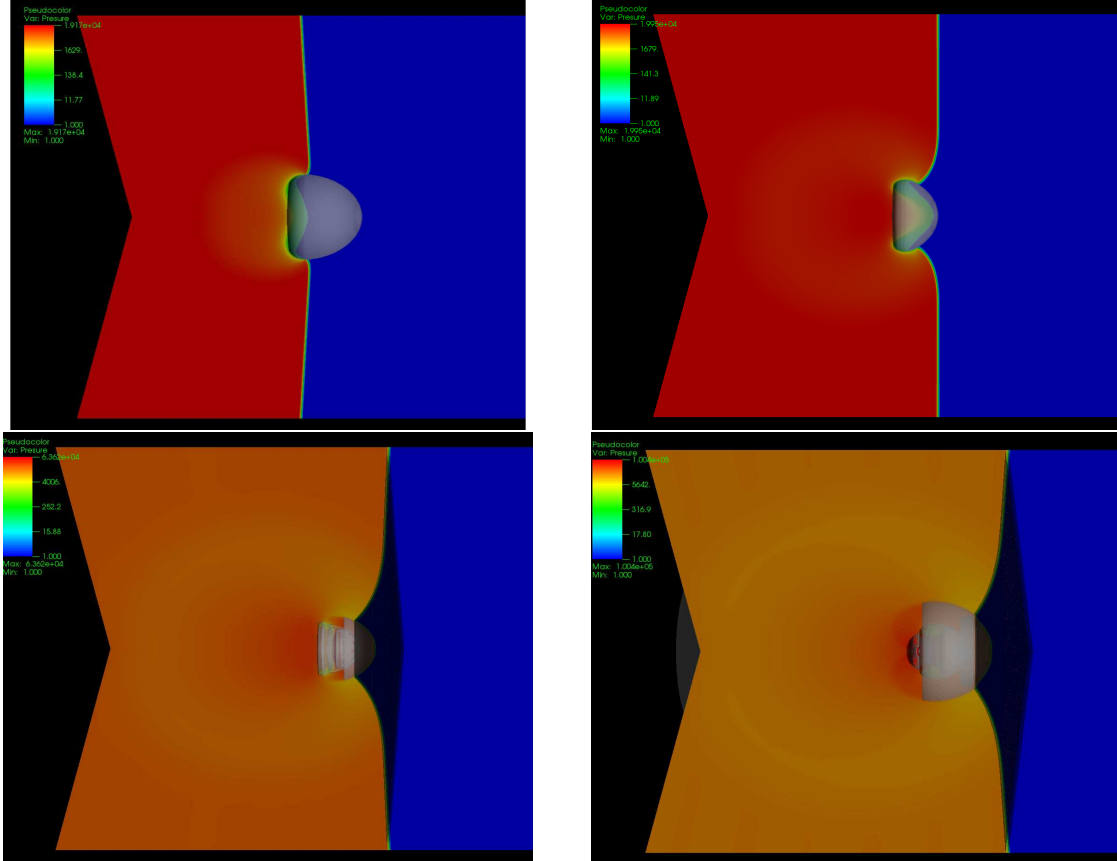
Figure 3: Evolution of the pressure (in bar) at different times t=2, 3.4, 3.8 and 4.2 μs. 3D simulation.

The evolution of the maximum pressure during the cavity collapse is plotted in Figure 1 (right part) for both 2D and 3D simulations. We can observed the first peak after the water jet impacts the bubble front and the second peak (more intense) when the leftward blast wave collides the bubble fragments. As observed previously [4], the collapse process of a spherical bubble is faster and more intense, resulting in higher pressure peaks. Table 1 compares various quantitative measures between 2D and 3D simulations. The more intense peak reaches 111000 bar for the 3D case (50% more than the 2D collapse). These effects are due to the higher focusing that the 3D situation entails, which lead to a faster water jet.

5   3D BUBBLE COLLAPSE NEAR A WALL

The second test is an extension of first one considering a wall placed behind the bubble at an initial distance from the center L. The ratio L/R is a major parameter that governs the bubble collapse dynamics. As suggested in [5], the bubble initially located at

a distance lower than $L/R = 2$ presents high potential to cause damage. We consider the case for which the distance $L = 5$ mm ($L/R = 1.66$). Numerical parameters are similar to the previous case. The size of the computational domain is $14 \times 12 \times 12$ mm and the mesh contains $1150 \times 800 \times 800$ cells. Due to the stiffness of the case, the time step is decreased to 10^{-10} s.

Three-dimensional views of the bubble are given in figure 4 where is plotted the pressure field (in bar) at different times. At time $t= 3.25\ \mu$s, the jet has collided the right interface generating the intense blast wave. At time $t= 3.6\ \mu$s, the incident shock impacts the wall and the bubble breaks into two parts. The bubble takes the shape of a vortex ring and convects towards the wall.
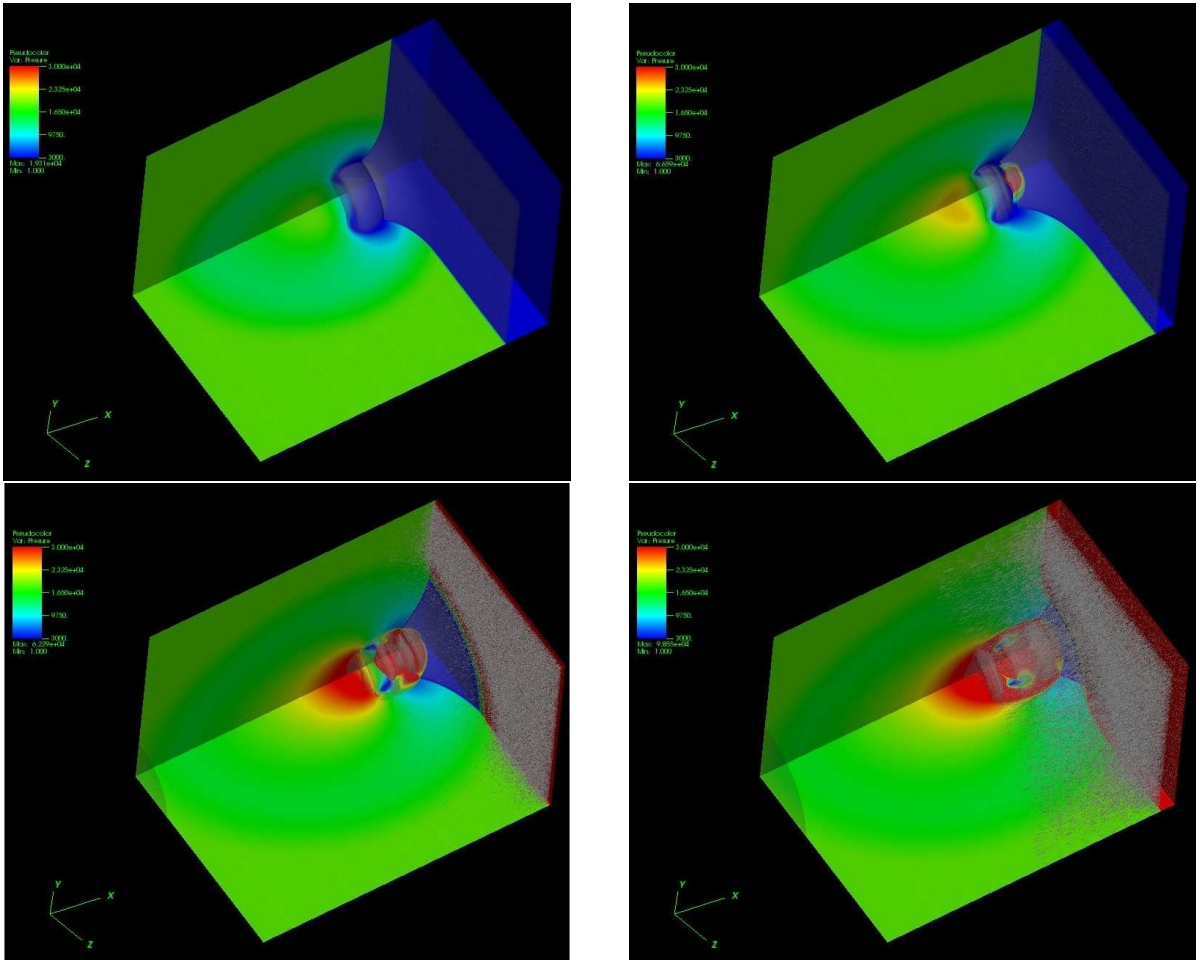
Figure 4: Evolution of the pressure (in bar) at different times $t=2.8, 3.25, 3.6$ and $3.8\ \mu s$. 3D simulation.

The pressure evolution along the wall is given in Figure 5 at different times. The axis is represented by the left corner. The size of the square is 7.5×7.5 mm. First, the incident shock wave impacts the wall (time $t= 3.6\ \mu$s). A peak (around 100000 bar) is observed on the axis when the rightward blast front impacts the wall (time $t= 3.8\ \mu$s) and reflects
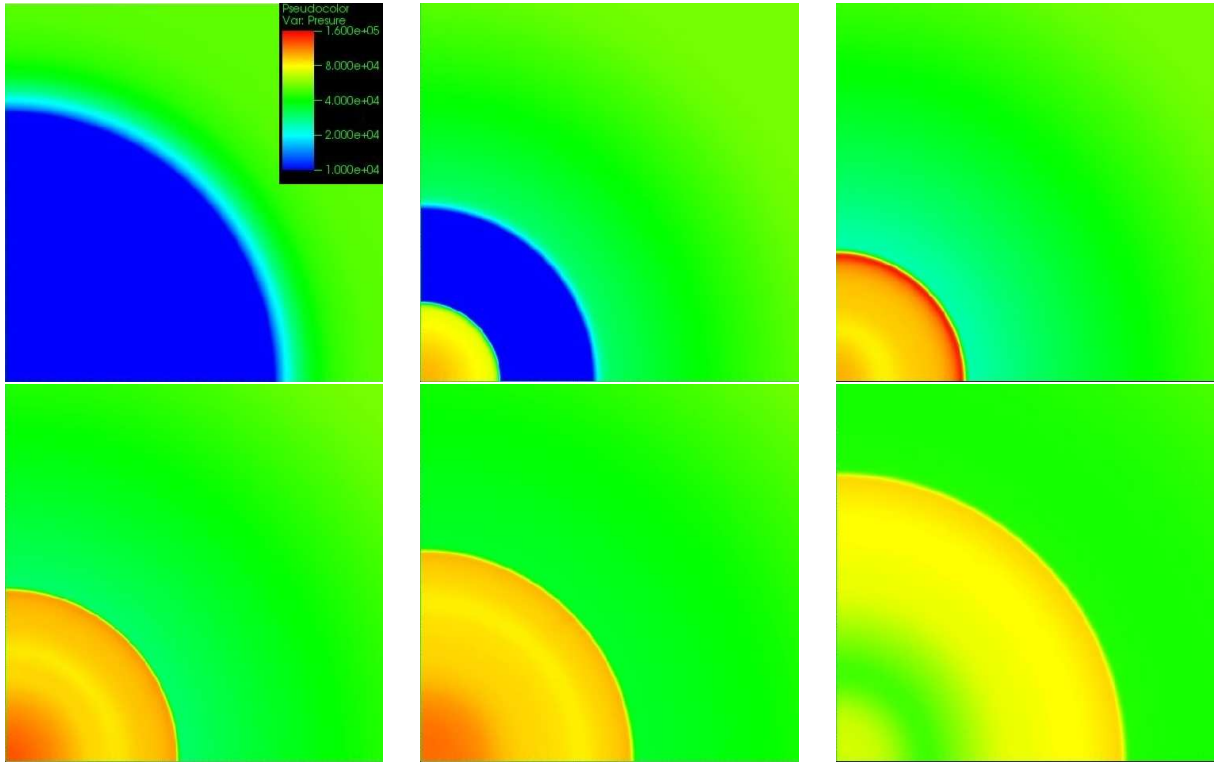
Figure 5: Evolution of the wall pressure (in bar) at different times t=3.6, 3.8, 4, 4.15, 4.3 and 4.65 μs. 3D simulation.

as a reinforced shock wave generating a very high-pressure area. The maximum value (around 150000 bar at a distance 2.5 mm from the axis) is due to this reflected wave and its focus with the spherical blast front at time t= 4 μs. At time t= 4.15 μs, another peak is observed along the axis (around 127000 bar) in the region near the throat formed by the bubble torus. In addition, many other pressure peaks are observed due to multiple wave reflections between the wall and the bubble. It suggests extensive regions of high pressure, which could induce stresses and thus a potential damage on the material.
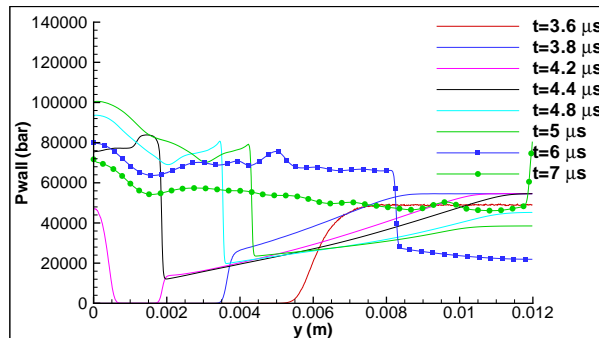
Figure 6: Evolution of the pressure along the wall. 2D simulation

In comparison, the pressure evolution along the wall obtained from the 2D simulation

is plotted in Figure 6. At time $t= 4.2\mu$s, the blast wave impacts the wall. A high-pressure are is generating by the reflected wave (time $t= 4.4\mu$s) which propagates toward the bubble. The maximum value (around 100000 bars) is reached along the axis at time $t= 5$ μs. The intensity for the 3D collapse is therefore 50% more than the 2D case and the location of the maximum value on the wall is not the same.

6 CONCLUSIONS

A three-dimensional compressible one-fluid tool is used to simulate a spherical gas bubble collapse near a wall. The distance from the bubble center is $L/R = 1.66$. It is observed that a region of high-pressure is created after the blast wave reflects on the wall. This high-pressure area is not located along the axis but at a distance smaller than the bubble radius. In comparison with a 2D simulation, the pressure peak on the wall is 50% more intense. In future work, we plan to study the wall distance effect.

ACKNOWLEDGEMENTS

REFERENCES

[1] Bourne, N.K. On the collapse of cavities, *Shock Waves*(2002) **11**:447–455.

[2] Goncalves, E. and Charriere, B. Modelling for isothermal cavitation with a four-equation model. *Int. J. Multiphase Flow* (2014) **59**:54–72.

[3] Goncalves, E. and Zeidan, D. Simulation of compressible two-phase flows using a void ratio transport equation. *Commun. Comput. Phys.* (2018) **24**(1):167–203.

[4] Hawker, N.A., Ventikos, Y. Interaction of a strong shockwave with a gas bubble in a liquid medium: a numerical study. *J. Fluids Mech.* (2012) **701**:59-1797.

[5] Johnsen, E. and Colonius, T. Numerical simulations of non-spherical bubble collapse. *J. Fluids Mech.* (2009) **629**:231–262.

[6] Kapila, A.K., Menikoff, R., Bdzil, J.B., Son, S.F. and Stewart, D.S. Two-phase modeling of deflagration-to-detonation transition in granular materials: reduced equations. *Phys. Fluids* (2001) **13**:3002–3024.

[7] Lauer, E., Hu, X., Hickel, S. and Adams, N. Numerical modelling and investigation of symmetric and asymmetric cavitation bubble dynamics. *Comput. Fluids* (2012) **69**:1–19.

[8] Nourgaliev, R.R., Dinh, T.N. and Theofanous, T.G. Adaptive characteristics-based matching for compressible multifluid dynamics. *J. Comput. Phys.* (2006) **213**:500–529.

[9] Ozlem, M., Schwendeman, D.W. and Kapila, A.K. A numerical study of shock-induced cavity collapse. *Shock Waves* (2012) **22**:89–117.

[10] Plesset, M., Chapman, R. Collapse of an initially spherical vapour cavity in the neighbourhood of a solid boundary. *J. Fluids Mech.* (1971) **47**:283–290.

[11] Turangan, C.K., Jamaluddin, A.R., Ball, G.J. anfd Leighton, T.G. Free-Lagrange simulations of expansion and collapse of air bubbles *J. Fluids Mech.* (2008) **598**:1–25.